Bioconjugate Chemistry

Article

pubs.acs.org/bc

Nanoparticle PET/CT Imaging of Natriuretic Peptide Clearance Receptor in Prostate Cancer

Eric D. Pressly,[†] Richard A. Pierce,[‡] Luke A. Connal,[†] Craig J. Hawker,[†,#] and Yongjian Liu*[,§]

[†]Materials Research Laboratory and [#]Materials Department and Department of Chemistry, and Biochemistry, University of California, Santa Barbara, California 93106, United States

[‡]Department of Medicine and [§]Department of Radiology, Washington University, St. Louis, Missouri 63110, United States

Supporting Information

ABSTRACT: Atrial natriuretic peptide has been recently discovered to have anticancer effects via interaction with cell surface natriuretic peptide receptor A (NPRA) and natriuretic peptide clearance receptor (NPRC). In a preclinical model, NPRA expression has been identified during tumor angiogenesis and may serve as a potential prognostic marker and target for prostate cancer (PCa) therapy. However, the presence of NPRC receptor in the PCa model has not yet been assessed. Furthermore, there is still no report using nanoparticle for PCa positron emission tomography (PET) imaging. Herein, an amphiphilic comb-like nanoparticle was synthesized with controlled properties through modular construction containing C-atrial natriuretic factor (CANF) for NPRC receptor targeting and 1,4,7,10-tetraazacyclododecane-1,4,7,10-tetraacetic acid (DOTA) chelator for high specific activity Cu-64 radiolabeling. The pharmacokinetics of ^{64}Cu-CANF-Comb exhibited tuned biodistribution and optimized in vivo profile in contrast to the nontargeted ^{64}Cu-Comb nanoparticle. PET imaging with ^{64}Cu-CANF-Comb in CWR22 PCa tumor model showed high blood pool retention, low renal clearance, enhanced tumor uptake, and decreased hepatic burden relative to the nontargeted ^{64}Cu-Comb. Immunohistochemistry staining confirmed the presence of NPRC receptor in tumor tissue. Competitive PET receptor blocking study demonstrated the targeting specificity of ^{64}Cu-CANF-Comb to NPRC receptor in vivo. These results establish a new nanoagent for prostate cancer PET imaging.

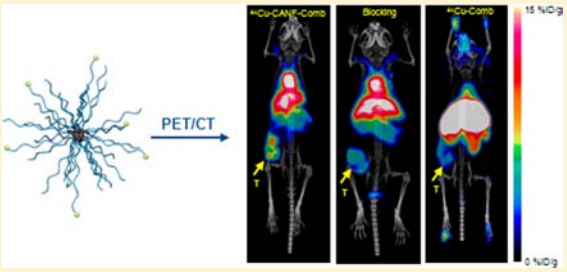

INTRODUCTION

Prostate cancer (PCa) is the most common noncutaneous malignancy affecting men in the U.S., with 241 740 estimated new cases resulting in approximately 28 170 deaths in 2012.[1] With the widespread use of screening tests (for example, prostate-specific antigen testing), patients are diagnosed with less-advanced disease, and the prostate-cancer-specific mortality has declined over the past few years. This has shifted the focus of treatment from whole-gland to focal therapy owing to the multifocal nature of prostate cancer.[2] Thus, specific and sensitive imaging becomes the key for early diagnosis, staging, and monitoring of treatment response.

Clinically, many imaging modalities have been used for PCa detection and staging including transrectal ultrasound, magnetic resonance imaging (MRI), computed tomography (CT), single photon emission computed tomography (SPECT), and positron emission tomography (PET).[3] Among them, MRI provides the highest spatial resolution and allows the best depiction of the internal zone anatomy of the prostate as well as its contours. Lately, with the advance of functional MRI such as dynamic contrast-enhanced MRI, MRI can also be used for PCa detection and staging.[4] However, radiotracer based imaging modalities, especially PET and PET/CT, are still favored owing to the high sensitivity and functional imaging which enables the early detection and monitoring of the physiological process during PCa development.[5] Currently, the most common radiotracer for clinical PET imaging, [^{18}F]-fluoro-2-deoxy-2-D-glucose ([^{18}F]-FDG), is not effective in the diagnosis of localized prostate cancer because of PCa's glucose independent metabolism.[6] Other tracers used for clinical research such as ^{18}F/^{11}C-choline or ^{11}C-acetate have shown promise in early studies, but the results need to be evaluated further in larger prospective clinical trials. Still, none of these tracers is PCa specific.

In the development of PET imaging probes for PCa, the majority of studies have focused on the use of small-molecule based tracers such as prostate-specific membrane antigen targeting molecules or gastrin-releasing peptide receptor targeted probes.[7−13] However, most of these had fast renal clearance and therefore low tumor uptakes, which may limit the potential for translational research. Nanoparticles, because of the unique physicochemical properties such as multivalency and multifunctionality, have been widely used for various cancer diagnosis and therapy[14−17] including PCa.[18−20] Currently, there are few studies of nanoagents for PCa PET imaging.

Received: August 27, 2012
Revised: December 11, 2012
Published: December 28, 2012

Natriuretic peptide is a group of cardiac hormones that play an important role in vasodilation, cardiovascular homeostasis, sodium excretion, and inhibition of aldosterone secretion by interacting with their receptors.[21] Additionally, they have been reported to have other physiologic effects such as involvement in immunity and inflammation. [22] Lately, atrial natriuretic peptide (ANP) has been reported to impart an anticancer effect via interaction with cell surface natriuretic peptide receptor A (NPRA) and natriuretic peptide clearance receptor (NPRC).[22−25] NPRA expression has been well characterized during the tumor angiogenesis process and might serve as a potential prognostic marker and target for PCa imaging and therapy.[22,25] Interestingly, NPRC receptor was also identified in human prostate carcinoma cells, and its gene expression was confirmed in mouse xenograft model.[26,27] Since the NPRC receptor population accounts for approximately 95% of all natriuretic peptide receptors, imaging the up-regulation of NPRC receptor in PCa model could identify a powerful target for early detection of PCa.

In the current study, a nanoparticle was designed and synthesized with a controlled loading of NPRC targeting peptide C-type atrial natriuretic factor (CANF) and 1,4,7,10-tetraazacyclododecane-1,4,7,10-tetraacetic acid (DOTA) chelator for ^{64}Cu radiolabeling. We have investigated the use of this well-defined polymeric nanoparticle for in vivo pharmacokinetic evaluation and PET imaging in a mouse CWR22 prostate tumor model. The targeting specificity and imaging efficiency were compared with the control nanoparticles and confirmed with the use of small-animal PET/CT. This work identifies the up-regulation of NPRC receptor in PCa model which may serve as a new biomarker for future targeted cancer therapy.

EXPERIMENTAL SECTION

Materials. Chemicals were purchased from Sigma-Aldrich (St. Louis, MO, USA) and used without further purification unless otherwise stated; functionalized poly(ethylene glycol) (PEG) derivatives were obtained from Intezyne Technologies, (Tampa, FL, USA). ^{64}Cu was prepared on the Washington University Medical School CS-15 Cyclotron by the ^{64}Ni-(p,n)^{64}Cu nuclear reaction at a specific activity of 50−200 mCi/μg (end of bombardment), as previously described.[35] The buffers used for ^{64}Cu-labeling were treated with Chelex-100 resin (Bio-Rad Laboratories, Hercules, CA, USA) before use. Tris-*t*-butylester-DOTA and 1,4,7,10-tetraazacyclododecane were purchased from Macrocyclics (Dallas, TX, USA). Centricon tubes (YM-30, MWCO 30 kDa; YM-50, MWCO 50 kDa; YM-100, MWCO 100 kDa) were purchased from Millipore. HiTrap Desalting columns (5 mL) were purchased from GE Healthcare Biosciences (Piscataway, NJ, USA). 2-(2-Bromoacetoxy)ethyl methacrylate,[36] dithiol ester radical addition−fragmentation transfer (RAFT) agent,[37] 1,4,7,10-tetraazacyclododecane-1,4,7-tris(*t*-butyl acetate) (DO3A),[38] and 4-pentynoic anhydride[39] were prepared as previously reported. Vitronectin, fibronectin, $\alpha_v\beta_3$, and $\alpha_v\beta_5$ were purchased from Chemicon. Integrin $\alpha_{IIb}\beta_3$ was purchased from EMD Chemicals, Inc. (Gibbstown, NJ).

Polymeric materials were characterized by ^{1}H and ^{13}C nuclear magnetic resonance (NMR) spectroscopy using a Bruker 200, 300, or 500 MHz spectrometer with the residual solvent signal as an internal reference. Gel permeation chromatography (GPC) was performed in DMF on a Waters system (Millford, MA, USA) equipped with four 5-mm Waters columns (300 × 7.7 mm) connected in series with increasing pore size (10^2, 10^3, 10^4, and 10^6 Å). Waters 410 differential refractometer index and 996 photodiode array detectors were employed. The molecular weights of the polymers were calculated relative to linear poly(ethylene oxide) standards. Fourier transformed infrared spectroscopy was performed using a Nicolet Magna 850 IR-Raman instrument on a CaF_2 salt plate. The spectra were acquired at a 4 cm^{-1} resolution and 128 scans. A Bioscan 200 imaging scanner (Bioscan, Washington, DC, USA) was used to read the instant thin layer chromatography (ITLC) plates (Pall ITLC-SG plates, VWR International, Batavia, IL, USA). Fast protein liquid chromatography (FPLC) and radio-FPLC were performed using an ÄKTA FPLC system (GE Healthcare Biosciences) equipped with a Beckman 170 Radioisotope Detector (Beckman Instruments, Fullerton, CA, USA).

Synthesis of DOTA Methacrylate (DOTA-MA). DO3A (1.92 g, 3.74 mmol) and 2-(2-bromoacetoxy)ethyl methacrylate (1.02 g, 4.06 mmol) were dissolved in acetonitrile (50 mL) followed by the addition of K_2CO_3 (0.62 g, 4.48 mmol), and the reaction mixture was then stirred overnight at RT. Dichloromethane (50 mL) was added to the reaction which was extracted with water (25 mL), concentrated by rotary evaporation, and purified by flash chromatography (DCM/MeOH, 95:5) to obtain a viscous clear oil (yield 1.81 g, 71%); ^{1}H NMR (500 MHz, $CDCl_3$) δ 6.14 (s, 1H), 5.63 (s, 1H), 4.39 (d, J = 19.1 Hz, 4H), 3.98−2.05 (m, 22H), 1.96 (s, 3H), 1.47 (t, J = 6.7 Hz, 27H). The product was anayzed with ESI-TOF mass spectrometry. (m/z): [M]+ calcd. 684.43, $C_{34}H_{60}N_4O_{10}$; found 684.53.

Synthesis of Poly(Ethylene Glycol) Methyl Ether Methacrylate (PEGMA). 5.0 kDa poly(ethylene glycol) monomethyl ether (mPEG, 5.00 g, 1.00 mmol) was dissolved in dichloromethane (25 mL) and triethylamine (5 mL). Freshly distilled methacryloyl chloride (5.00 mL, 5.35 g, 5.12 mmol) was added dropwise at 0 °C and the reaction mixture was allowed to stir overnight under argon. The reaction was quenched with water, filtered, and the organic phase washed with 10% $NaHSO_4$ (w/v), dried over anhydrous $MgSO_4$, and concentrated in vacuum to ca. 10 mL. The product was precipitated by adding cold diethyl ether (200 mL) and dried in vacuum (4.65 g, 92%); ^{1}H NMR ($CDCl_3$, 200 MHz) δ 6.15 (1H), 5.58 (1H), 4.32 (2H), 3.6 (450H), 1.95 (2H); M_n = 5.1 kDa. PDI: 1.03.

Synthesis of Azido Poly(Ethylene Glycol) Methacrylate (N_3-PEGMA). 5.0 kDa poly(ethylene glycol) monoazide (1.50 g, 0.30 mmol) was dissolved in dichloromethane (15 mL) and triethylamine (3 mL). Freshly distilled methacryloyl chloride (0.70 mL, 0.75 g, 7.1 mmol) was added dropwise at 0 °C and the reaction mixture was allowed to stir overnight under argon. The reaction was quenched with water, filtered, and the organic phase washed with 10% $NaHSO_4$ (w/v), dried over anhydrous $MgSO_4$, and concentrated in vacuum to ca. 3 mL. The product was precipitated by adding cold diethyl ether (100 mL) and dried in vacuum (yield 1.11 g, 74%); ^{1}H NMR (500 MHz, CD_2Cl_2) δ 6.13 (s, 1H), 5.61 (s, 1H), 4.35−4.26 (m, 2H), 3.78−3.57 (m, 464H), 3.53−3.45 (m, 3H), 3.42 (t, J = 5.0 Hz, 2H), 1.97 (s, 3H); M_n = 5.1 kDa. PDI: 1.03.

Synthesis of Acteylene-CANF. CANF (59.3 mg, 0.037 mmol) was dissolved in 2 mL anhydrous DMF, and 4-pentynoic anhydride (19.2 mg, 0.098 mmol) dissolved in 1.5 mL anhydrous DMF was added dropwise to the solution and allowed to stir 2 days. Cold diethyl ether (15 mL) was added to the solution to triturate the product, which was subsequently

dx.doi.org/10.1021/bc300473x | *Bioconjugate Chem.* 2013, 24, 196−204

dissolved in 2 mL of Milli-Q water and freeze−dried (yield 47.0 mg, 75%); M_w(ESI) 1674.73 {M+H$^+$] (calc. 1674.80).

Synthesis of Poly(Ethylene Glycol) CANF Methacrylate (CANF-PEGMA). N_3−-PEGMA (75.4 mg, 0.015 mmol) and Acetylene-CANF (42.8 mg, 0.025 mmol) were dissolved in a solution of 1.0 g DMSO and 0.65 g Milli-Q water followed by the additions of 50 μL 5 wt % aqueous copper sulfate (0.018 mmol) and 75 μL 5 wt % aqueous sodium ascorbate (0.016 mmol), respectively. The reaction was allowed to stir for two days with repeat additions of $CuSO_4$ (50 μL) and sodium ascorbate (75 μL) solutions after one day. The product was purified by washing (10×) with Milli-Q water in 15 mL centricon tubes (YM-5) and freeze−dried (yield 48 mg, 41%) (see Figure S1 for NMR (DMSO-d_6), FT-IR, ν (cm^{-1}): 3315, 2881, 1655, 1466, 1342, 1099, 962, 841. GPC M_n 6500, PDI 1.1 (PMMA standards, DMF).

Synthesis of Comb Copolymers. The synthesis of comb polymers was adapted from a previous report[29] with the exception of DOTA methacrylate and poly(ethylene glycol) CANF methacrylate being incorporated into the polymerization mixture. To illustrate, PEGMA 5.0 kDa (205 mg, 0.041 mmol), CANF-PEGMA (100 mg, 0.015 mmol), methyl methacrylate (MMA) (43.6 mg, 0.51 mmol), azobisisobutyronitrile (AIBN) (0.069 mg, 0.00042 mmol), DOTA-MA (22.2 mg, 0.032 mmol), and RAFT agent (0.33 mg, 0.0011 mmol) were dissolved in DMF (1.99 g). AIBN, DOTA-MA, and RAFT agent were added as DMF stock solutions. The solution was transferred to a 5 mL Schlenk flask and three freeze−pump−thaw cycles performed before being heated at 70 °C for 120 h. Following the polymerization, the solution was diluted with DMF, transferred to four 15 mL centricon tubes (YM-50), and extensively washed with DMF, removal of monomers monitored by GPC. The copolymer was then washed with Milli-Q water (5×) and freeze−dried to give the desired graft copolymer as a white powder (yield 68 mg); M_n = 205 kDa, PDI 1.20, and M_n = 220 kDa, PDI 1.25, for CANF-Comb and control Comb, respectively (GPC-DMF, PMMA standards).[28]

DOTA Deprotection and Formation of Nanoparticles. After removal of *t*-butyl protecting groups,[29] the polymers were dissolved in DMSO (1 wt %), a rapid addition of an equal aliquot achieved assembly, and DMSO was removed by centrifugal filtration, resulting in particles of 16 and 22 nm (dynamic light scattering) for the targeting CANF-Comb (zeta potential: −1.1 ± 1 mV) and nontargeting Comb (zeta potential: −35 ± 4 mV) particles, respectively (Scheme 1). After centrifugal filtration cycles with Milli-Q water (3×), the nanoparticles were reconstituted in water (ca. 3 mg/mL) and stored at 4 °C for further use.

CWR22 Mouse Prostate Cancer Model. All animal studies were performed in compliance with guidelines set forth by the NIH Office of Laboratory Animal Welfare and were approved by the Washington University Animal Studies Committee. CWR22 model, an androgen dependent xenograft model derived from a primary human prostatic carcinoma,[30] has been widely used for various PCa treatment studies.[31,32] Since the purpose of this study was to identify NPRC as a new PCa biomarker for PET imaging and serve as a foundation for future targeted therapy study, the CWR22 model was selected. Briefly, 4- to 6-week-old athymic nu/nu male mice were obtained from Charles River Laboratories. The CWR22 tumor line was a gift from Dr.Thomas G. Pretlow (Case Western Reserve University, Cleveland, OH). The CWR22 tumor was propagated in the animals by the implantation of minced tumor

Scheme 1. (A) Synthesis of CANF-PEG-Methacrylate Monomer via "Click" Chemistry. (B) Synthesis of CANF-Comb, Deprotection, and Subsequent Assembly into Nanoparticles

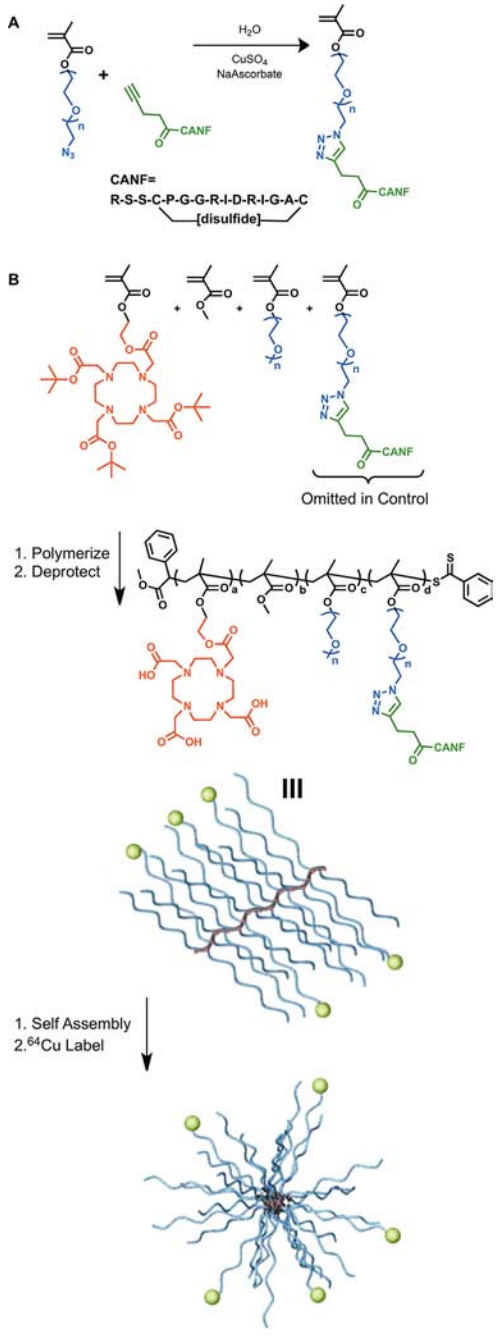

tissue, from a previously established tumor, into the subcutaneous tissue of the right flank of the mice.[33] Six to eight weeks after implantation, the tumor grew to about 700−1000 mm^3, and then the mice were injected intravenously with the developed nanoparticles. The growth curve of the CWR22 tumor bearing mice was illustrated in Figure S2.

Copper-64 Radiolabeling of CANF-Comb and Comb. The ^{64}Cu (half-life = 12.7 h, β^+ = 17%, β^- = 40%) was produced at the Washington University cyclotron facility by the ^{64}Ni (p,n) ^{64}Cu nuclear reaction at a specific activity of 1.85−7.40 GBq/μg at the end of bombardment.[34,35] The Cu-64 radiolabeling procedure for the two nanoparticles followed the

dx.doi.org/10.1021/bc300473x | *Bioconjugate Chem.* 2013, 24, 196−204

reported procedure. Briefly, the targeted CANF-Comb and nontargeted Comb (5 μg, about 5 pmol) were incubated with 185 MBq ^{64}Cu in 200 μL 0.1 M pH 5.5 ammonium acetate buffer at 80 °C for 1 h, respectively. After ethylene diamine tetraacetic acid (EDTA, 10 mM in 50 mM pH 7.4 phosphate buffer) challenge, the ^{64}Cu-CANF-Comb and ^{64}Cu-Comb were separated from ^{64}Cu-EDTA with 2 mL zeba spin desalting column. The radiochemical purity of the labeled nanoprobe was measured by radioactive thin layer chromatography (Radio-TLC) (Washington, DC).

Biodistribution Studies. ^{64}Cu-CANF-Comb and ^{64}Cu-Comb were reconstituted in 0.9% sodium chloride (APP pharmaceuticals) for intravenous (i.v.) injection. Male CWR22 mice weighing 25−32 g (n = 24) were anesthetized with inhaled isoflurane, and about 370 kBq of labeled nanoparticles (~4.0 μg/kg body weight) in 100 μL saline were injected via the tail vein. The mice were re-anesthetized before euthanizing them by cervical dislocation at each time point (1 h, 4 h, and 24 h) post injection (p.i.). Organs of interest were collected, weighed, and counted in a well gamma counter (Beckman 8000, San Diego, CA). Standards were prepared and measured along with the samples to calculate the percentage of the injected dose per gram of tissue (%ID/gram) or percentage of the injected dose per organ of tissue (%ID/organ).[36]

PET/CT Imaging. About 6 weeks after the tumor implantation, CWR22 tumor-bearing mice were anesthetized with isoflurane and injected i.v. with 3.7 MBq/100 μL of ^{64}Cu labeled nanoparticles via the tail vein. The microPET images (corrected for attenuation, scatter, normalization, and camera dead time) sessions were carried out on an Inveon PET/CT system (Siemens Medical Solutions, Knoxville, TN) and microPET Focus 220 at 1 h (one 15-min frame), 4 h (one 30-min frame), and 24 h p.i. (one 60-min frame). All the PET scanners were cross-calibrated periodically. The microPET images were analyzed with ASIPro.[37] The tumor uptake of ^{64}Cu-CANF-Comb was calculated in terms of the mean standardized uptake value (SUV) in three-dimensional (3D) regions of interest (ROIs). In general, SUV is defined as the tissue concentration of radiotracer divided by the activity injected per body weight and is calculated according to the following equation. The SUV data were not corrected for partial volume effects.[38]

$$\mathrm{SUV} = \frac{\text{radioactivity concentration in ROI[Bq/mL]}}{\text{injected}\dfrac{\text{dose[Bq]}}{\text{animal weight[g]}}}$$

After the PET imaging, the animals were euthanized by cervical dislocation and the tumors were fixed in situ with freshly prepared 4% paraformaldehyde (Electron Microscopy Science Inc., Hatfield, PA) for histopathology and immunohistochemistry.

Competitive Receptor Blocking Studies. Competitive PET receptor blocking studies were performed in CWR22 tumor-bearing mice (27.9 ± 2.9 g) with coinjection of nonradiolabeled CANF-Comb and ^{64}Cu-CANF-Comb with 100:1 mol ratio for both biodistribution and PET/CT imaging studies.

Immunohistochemistry. Tumor tissue specimens were fixed in the 4% paraformaldehyde right after collection, stored overnight at 4 °C, and then embedded in paraffin and sectioned at 5 μm for immunohistochemistry. Following dewaxing and hydration, sections were heated in 10 mM sodium citrate pH 6.0 with 0.1% Tween for 15 min at boiling temperature for antigen retrieval. Following blocking with nonimmune serum, sections were incubated with Genway (San Diego, CA) mouse monoclonal anti-NPRC antibody 4C3 overnight at 1:400 dilution using Vector Laboratories M.O.M. kit (Burlingame, CA). Color development employed Vector Laboratories Vectastain alkaline phosphatase ABC system (Burlingame, CA) and blue substrate, and sections were counterstained using nuclear fast red. Sections incubated with preimmune serum and sections incubated with secondary antibody only gave no signal.

Statistical Analysis. Group variation is described as mean ± standard deviation. Group comparisons were made using Student t test. The significance level in all tests was $p \leq 0.05$. GraphPad Prism v 5.02 (La Jolla, CA) was used for all statistical analyses.

RESULTS

Biodistribution in CWR22 Tumor-Bearing Mice. Biodistribution results of the nontargeted nanoparticle ^{64}Cu-Comb in CWR22 tumor mice showed similar pharmacokinetics as were reported previously (Figure 1A in %ID/g, Figure S3A in %ID/organ).[39] The blood retention of ^{64}Cu-Comb showed a decreasing profile from 24.6 ± 1.41%ID/g at 1 h p.i. to 8.28 ± 0.20% ID/g at 24 h. The liver uptakes were dominant during the whole study and increased over time from 25.8 ± 6.47%ID/g at 1 h to 37.1 ± 9.02%ID/g at 24 h. Interestingly, spleen accumulation dropped to about half of the initial uptake by 24

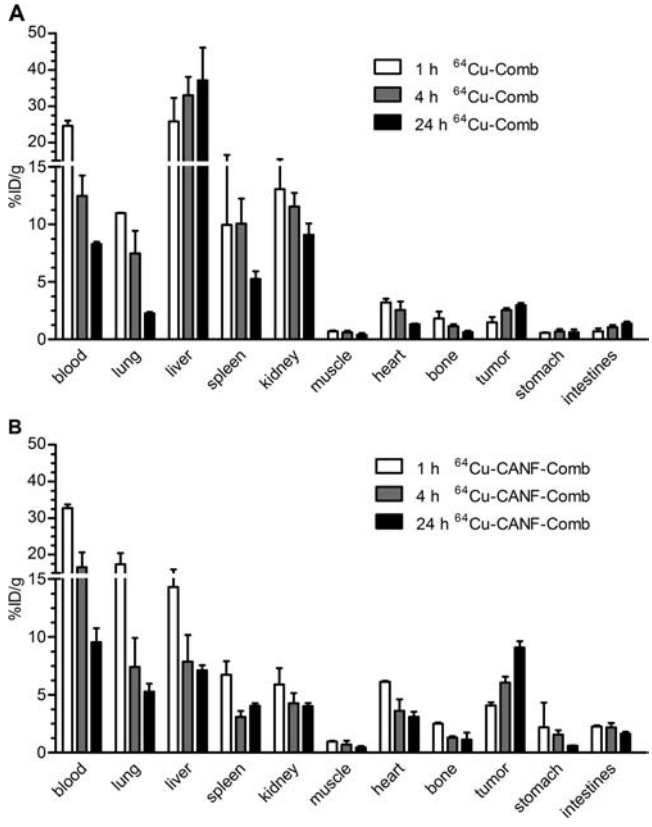

Figure 1. Biodistribution of ^{64}Cu-Comb and ^{64}Cu-CANF-Comb in CWR22 tumor model following intravenous injection (n = 4/group). (A) ^{64}Cu-Comb showing low tumor accumulation but high liver uptake. (B) ^{64}Cu-CANF-Comb showing high tumor localization and superior pharmacokinetics relative to ^{64}Cu-Comb with high blood retention and low hepatic burden.

dx.doi.org/10.1021/bc300473x | Bioconjugate Chem. 2013, 24, 196−204

h. The other clearance of ^{64}Cu-Comb was through the kidney with ~10% ID/g across the study, relative to the low accumulation in gastrointestinal tract (stomach and intestines). Tumor uptake almost doubled during the 24 h study, which led to increased tumor-to-muscle (T/M) ratio and tumor-to-blood (T/B) ratio from 2.10 ± 0.72 and 0.06 ± 0.02 at 1 h to 7.50 ± 2.09 and 0.36 ± 0.02 at 24 h, respectively.

The targeted ^{64}Cu-CANF-Comb showed a biodistribution profile superior to that of the nontargeted ^{64}Cu-Comb during the 24 h study (Figure 1B in %ID/g, Figure S3B in %ID/organ). In contrast to the high and gradually increased reticuloendothelial system (RES) clearance of ^{64}Cu-Comb, the liver accumulation of ^{64}Cu-CANF-Comb progressively decreased during the study. At each time point, the liver accumulations of ^{64}Cu-CANF-Comb were all significantly (p < 0.05, n = 4) lower than those of nontargeted ^{64}Cu-Comb. Especially at 24 h, the liver uptake of ^{64}Cu-CANF-Comb was only 15% of that obtained with ^{64}Cu-Comb. Also, the blood retentions of ^{64}Cu-CANF-Comb were all higher (p < 0.0001 at 1 h, n = 4) than those of ^{64}Cu-Comb at each time point. More importantly, the tumor showed increasing localization of ^{64}Cu-CANF-Comb over time. The tracer uptake SUVs, T/M ratios, and T/B ratios (0.12 ± 0.01, 0.36 ± 0.09, and 0.95 ± 0.13 at 1, 4, and 24 h, respectively) at each time point were all significantly (p < 0.001, n = 4) higher than those obtained with the nontargeted ^{64}Cu-Comb.

PET/CT Imaging. PET/CT images at 24 h clearly showed the tumor accumulation of ^{64}Cu-CANF-Comb in CWR22 tumor bearing mice, in contrast to the weak tumor accumulation observed with nontargeted ^{64}Cu-Comb (Figure 2). Interestingly, the bladder accumulation was very low for

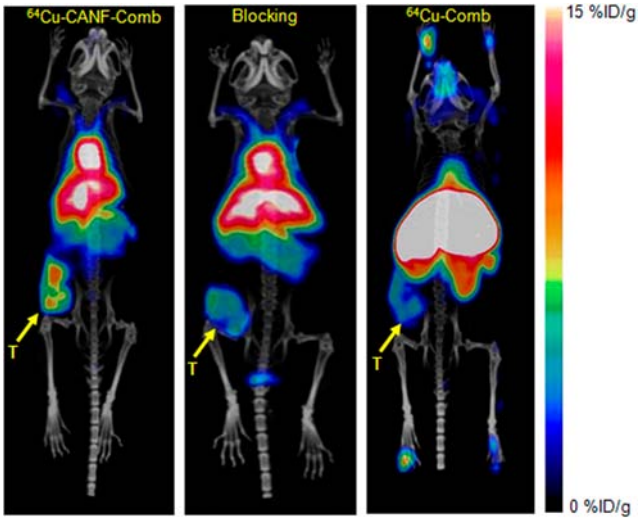

Figure 2. PET/CT images of ^{64}Cu-CANF-Comb, ^{64}Cu-CANF-Comb blocking, and ^{64}Cu-Comb in CWR 22 tumor at 24 h post injection. T: tumor.

both ^{64}Cu-CANF-Comb and ^{64}Cu-Comb. Consistent with the biodistribution results, ^{64}Cu-CANF-Comb showed higher heart accumulation and lower liver uptake than those obtained with ^{64}Cu-Comb. The quantitative analysis showed increased ^{64}Cu-CANF-Comb tumor localization over time (Figure 3A). At each time point, the tumor uptake and T/M ratio were all significantly (p < 0.05, n = 6–8) higher than corresponding data obtained with the nontargeted ^{64}Cu-Comb. Particularly at

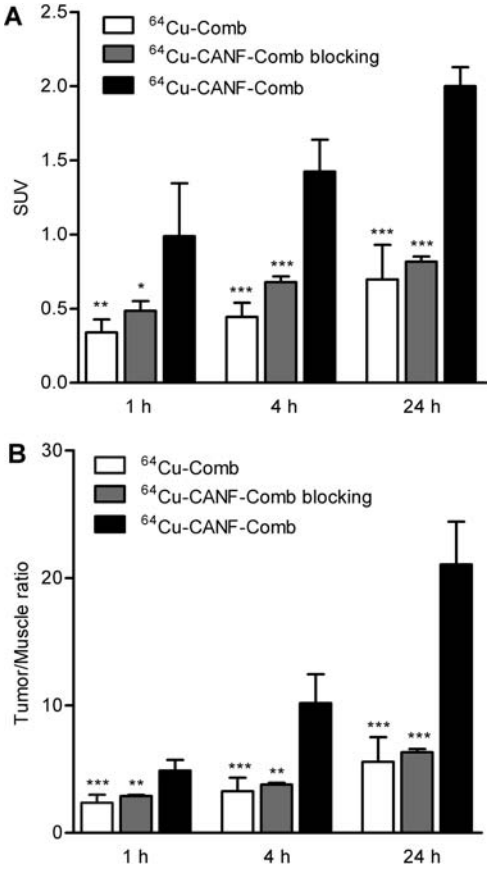

Figure 3. Quantitative tumor uptake SUVs (A) and tumor/muscle ratios (B) of ^{64}Cu-Comb, ^{64}Cu-CANF-Comb, and ^{64}Cu-CANF-Comb blocking in CWR 22 tumor at three different time points (n = 6–8/group) (statistical analysis of ^{64}Cu-Comb and ^{64}Cu-CANF-Comb blocking compared to ^{64}Cu-CANF-Comb; * p < 0.05; ** p < 0.001; *** p < 0.0001).

24 h, ^{64}Cu-CANF-Comb had a 3-fold greater T/M ratio than the nontargeted ^{64}Cu-Comb (Figure 3A,B).

Competitive Receptor Blocking. Competitive receptor blocking with coinjection of unlabeled CANF-Comb resulted in a substantial tumor uptake decrease while retaining similar in vivo pharmacokinetics profile. The organ uptakes (except for tumor) of the blocked group were all comparable to those obtained without blockade (Figure 4 in %ID/g, Figure S4 in %

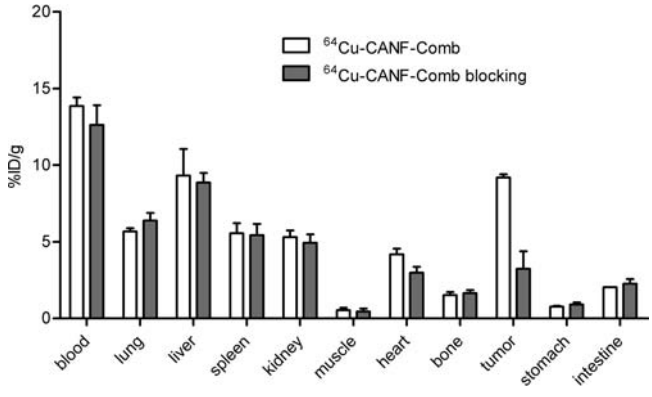

Figure 4. Biodistribution of ^{64}Cu-CANF-Comb and ^{64}Cu-CANF-Comb blocking in CWR 22 tumor model at 24 h post injection (n = 4/group, blockade:^{64}Cu-CANF-Comb = 100:1).

dx.doi.org/10.1021/bc300473x | Bioconjugate Chem. 2013, 24, 196–204

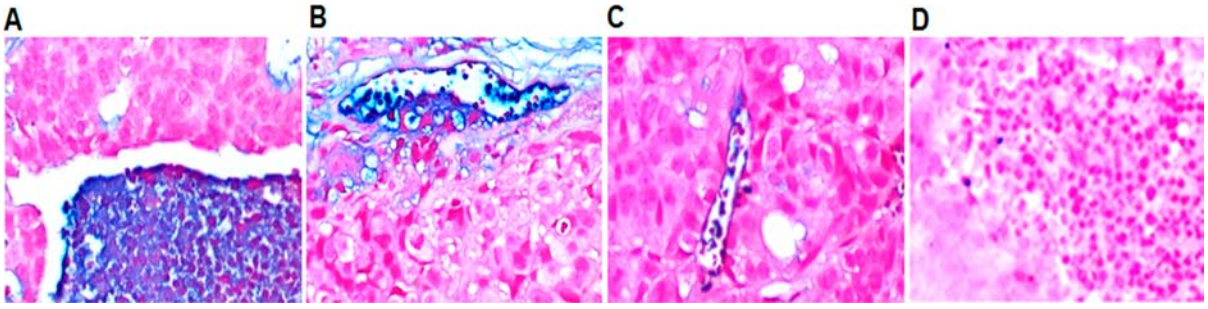

Figure 5. Immunohistochemical staining of NPRC receptor (blue) in tumor tissue (counterstained with nuclear fast red). (A) High expression of NPRC in pools of inflammatory cells within the tumor. (B) NPRC found in inflammatory cells and in the endothelial lining of small vessels in the tumor periphery. (C) NPRC staining of the endothelial wall and some inflammatory cells in a peripheral vessel within the tumor. (D) Section incubated with preimmune serum instead of primary antibody. All panels are at 200×.

ID/organ). However, the tumor accumulation was significantly ($p < 0.0001$, $n = 6$) blocked from 9.19 ± 0.21%ID/g to 3.23 ± 1.15%ID/g. Consistent with biodistribution blocking data, PET/CT image also clearly demonstrated the decreased tumor localization of ^{64}Cu-CANF-Comb (Figure 2). The quantitative analysis showed that the tumor uptake and T/M ratio were both significantly ($p < 0.01$, $n = 6$) reduced at each time point in the blocking group (Figure 3B).

Immunohistochemistry. Immunohistochemistry (IHC) showed the presence of cells positive for NPRC within and surrounding the tumor mass (Figure 5). The tumor cells were largely negative, but pools of NPRC positive inflammatory cells were found within the tumors (Figure 5A,B) and lining blood vessels in stromal tissue surrounding the tumors (Figure 5B,C). The control staining using a preimmune serum instead of primary antibody confirmed the specificity of NPRC IHC (Figure 5D).

■ DISCUSSION

Herein, we have reported the synthesis, characterization, and biological evaluation of ^{64}Cu-CANF-Comb, a nanoparticle for specific targeting of the NPRC receptor in human prostate cancer xenograft using in vivo biodistribution assay, small animal PET/CT imaging, as well as immunohistochemistry. This targeted nanoparticle exhibited improved pharmacokinetics with extended blood retention and low hepatic burden compared to the nontargeted ^{64}Cu-Comb nanoparticle. PET/CT imaging clearly showed the tumor uptake and confirmed the targeting specificity with blocking studies. The expression of NPRC receptor in tumor was also verified by IHC.

Radiolabeled peptides have been an effective way to target cellular receptors for in vivo diagnosis, characterization, and targeted radiotherapy owing to the high sensitivity and specificity.[9] In PCa imaging, gastrin-releasing peptide receptor has been widely studied with bombesin analogs for PET.[7,8,10,13,40] However, most of these tracers have low tumor uptakes due to the fast renal clearance. Among them, ^{64}Cu-SarAr-SA-Aoc-bombesin (7−14) had the highest tumor uptake (~13%ID/g and ~7%ID/g at 1 and 24 h, respectively) in all the ^{64}Cu labeled bombesin analogues.[7] Although the fast renal clearance lessened the concern of toxicity, it also led to low tumor/kidney (T/K) ratio (bladder was not collected), which might be an issue in further translational studies owing to possible interference on prostate tumor uptake quantification caused by high bladder accumulation of the radiotracer. Thus, an imaging probe with tuned in vivo pharmacokinetics and renal clearance, improved tumor uptake, and enhanced tumor-to-background ratio is necessary for clinical settings.

Nanoparticles, owing to the versatile physiochemical properties, can provide significant improvements in pharmacokinetics, targeting efficiency, and specificity for oncological diagnosis, potentially leading to earlier detection and better treatment options for cancer.[41] In the design of nanoparticles for targeted cancer diagnosis, the controlled structure including size, surface properties, targeting group, and radiolabeling site are important factors for in vivo imaging applications. In previous studies, the poly(methyl methacrylate)-core/PEG-shell amphophilic CANF-Comb nanoparticle has shown that its in vivo imaging capability could be accurately tailored by changing the molecular parameters of the starting functionalized copolymer.[39] Feed ratios were used to control the incorporation of various monomers, as methacrylate has been shown to copolymerize randomly.[29] The DOTA chelator for ^{64}Cu and CANF targeting peptide could be precisely conjugated to the Comb nanoparticles (~105 DOTA/particle) to have controlled radiolabeling specific activity and targeting efficiency. In this study, CANF peptide end functionalized onto a PEG macromonomer was copolymerized with a nonfunctional PEG macromonomer to afford comb-like copolymers; these polymers were self-assembled in water to afford CANF-Comb nanopartilces with high CANF loading (~35 CANF/particle) for initial evaluation (Scheme 1). As previously reported, higher loading of targeting peptide would decrease the systemic circulation of nanoparticles. Although the 25% CANF-Comb nanoparticles used in this study had similar size and surface charge to those used in the previous study (10% CANF-Comb, 14 CANF/particle), its 1 h blood retention was about 60% of the 10% CANF-Comb nanoparticle despite the difference in animal species, reasonably owing to the conjugation of ~21 more CANF peptide (150% higher loading), which was also confirmed by the change of octanol−water distribution coefficient (log P) from −2.03 ± 0.02 (10% CANF-Comb, $n = 4$) to less hydrophilic value of −1.47 ± 0.03 (25% CANF-Comb, $n = 4$). This clearly showed the advantage of using this poly(methyl methacrylate)-core/PEG-shell amphophilic nanoparticle to achieve tuned in vivo behavior through changing the molecular parameters of the starting functionalized copolymer.[39]

Previous studies had shown that neutral nanoparticles had extended in vivo blood retention and reduced hepatic and splenic accumulation compared to charged nanoparticles of similar size.[14] Herein, the surface charge effect was clearly illustrated. Compared to the neutral particle CANF-Comb

dx.doi.org/10.1021/bc300473x | Bioconjugate Chem. 2013, 24, 196−204

(−1.1 ± 1 mV), the negatively charged Comb nanoparticles (−35 ± 4 mV) showed less blood retention and gradually increased hepatic uptake during the 24 h study. For nanoparticle tumor targeting, one advantage is the well-known enhanced permeation and retention (EPR) effect due to the leaky vasculature of tumor and the size of nanoparticles, which was clearly observed for the nontargeted Comb nanoparticle with gradual increase over time (Figure 3). Although the elevated blood retention of CANF-Comb would cause greater EPR effect in tumor uptake compared to the Comb nanoparticle, the accumulation of CANF-Comb in CWR22 tumor was largely due to the active targeting to the NPRC receptor, as confirmed by the higher CANF-Comb/Comb tumor uptake ratios (2.4−3.1) than those of blood retention (1.2−1.3). Further, the biodistribution blocking studies also verified the NPRC receptor specific uptake, which showed similar ^{64}Cu-CANF-Comb uptakes in all the organs except for 2-fold decrease in tumor due to the nonradiolabeled CANF-Comb blockade. In the PET imaging study, the high specific activity (3.7 ± 1.1 GBq/nmol) of ^{64}Cu-CANF-Comb ensured only picomole level of radiotracer for in vivo application and minimal self-blocking effect, leading to high contrast and accurate quantification. The ^{64}Cu-CANF-Comb PET image clearly showed the high tumor localization and low liver accumulation (Figure 2). For the nontargeted ^{64}Cu-Comb nanoparticle, although tumor uptake was observed and increased along the study period (Figures 2, 3), it is still significantly lower than that of ^{64}Cu-CANF-Comb at each time point. Again, the PET blocking study of ^{64}Cu-CANF-Comb, consistent with the biodistribution study, clearly showed the substantial decrease in tumor accumulation to a level similar to that of the nontargeted ^{64}Cu-Comb, indicating the NPRC mediated tumor uptake (Figures 2, 3). Interestingly, the heart accumulation of ^{64}Cu-CANF-Comb did not change significantly with CANF-Comb blockade, indicating the uptake in heart was mainly due to the blood pool retention. Compared to the other reported PCa PET tracer,[12] ^{64}Cu-CANF-Comb showed sufficient T/M ratio (21.0 ± 3.4, n = 6−8) at 24 h and a higher T/K ratio (2.3 ± 0.2, n = 6−8), indicating the advantage of nanoparticles for PCa imaging and the potential for translational research. Additionally, the higher T/M and T/B ratios of ^{64}Cu-CANF-Comb than those of ^{64}Cu-Comb and ^{64}Cu-CANF-Comb blocking at the three time points also confirmed the NPRC receptor-specific tracer accumulation.

Since the recently discovered anticancer property of ANP,[23−25] NPRA has been demonstrated as a potential prognostic marker and a target for PCa therapy. NPRC receptor, though traditionally viewed as a clearance receptor of natriuretic peptide, occupies a large population (>95%) of the NPR family and has recently been implicated in more pathophysiological roles in human diseases.[42] Although the presence of NPRC receptor was identified in human PC-3 prostate carcinoma cells and mouse KUCaP-2 xenograft model, there was a lack of information about its detailed characterization and localization in the tumor and potential for PCa diagnosis. In this study, IHC staining clearly showed the up-regulation of NPRC receptor in both tumor margin (possibly inflammatory cells and endothelial) and tumor interior (inflammatory cells) (Figure 5). The initial study of the NPRC positive inflammatory cells inside the tumor showed colocalization with CD31 (Figure S5), confirming the presence of NPRC receptor during tumor angiogenesis and indicating its important role as diagnostic biomarker for tumorigenesis.[43,44]

CONCLUSION

Through controlled synthesis and assembly, a CANF peptide conjugated polymeric nanoparticle was prepared with tuned physicochemical and biological properties for PCa PET imaging. Immunohistochemistry confirmed the up-regulation of NPRC receptor in this CWR22 tumor model. Initial in vivo evaluation demonstrated the superiority of targeted imaging over passive EPR effect in oncological diagnosis. The optimized in vivo pharmacokinetics, high sensitivity, and specificity make ^{64}Cu-CANF-Comb a candidate for PCa PET imaging.

ASSOCIATED CONTENT

Supporting Information

NMR of CANF-PEG-Methacryate monomer, CWR22 tumor growth curve, biodistribution histograms, histochemically stained images, and characterization data for nanoparticles. This material is available free of charge via the Internet at http://pubs.acs.org.

AUTHOR INFORMATION

Corresponding Author

*E-mail: liuyo@mir.wustl.edu. Phone: 314-362-8431. Fax: 314-362-9940.

Notes

The authors declare no competing financial interest.

ACKNOWLEDGMENTS

We thank Terry Sharp, Nicole Fettig, Margaret Morris, Amanda Roth, Lori Strong, and Ann Stroncek for their assistance with animal imaging studies; and Tom Voller, Paul Eisenbies, and Evelyn Madrid for ^{64}Cu production. We thank Dr. Farrokh Dehdashti for editing. This work was supported by the National Institutes of Health as a Program of Excellence in Nanotechnology (HHSN268201000046C) (E.P., R.P., L.A.C., C.J.H., and Y.L.) and the National Science Foundation through the MRSEC program (DMR-1121053 − E.P., L.A.C., and C.J.H.). We are grateful for funding support from Mallinckrodt Institute of Radiology, Washington University School of Medicine. The production of ^{64}Cu is supported by the National Cancer Institute (CA86307) with morphological studies and immunohistochemistry being supported by NIH/NHLBI PO1 HL29594. No other potential conflict of interest relevant to this article was reported.

DEDICATION

In memory of Professor Michael J. Welch, a leading PET imaging scientist and strong supporter of this research who passed away on May 6th, 2012.

ABBREVIATIONS

ANP, atrial natriuretic peptide; CANF, C-atrial natriuretic factor; CT, computed tomography; DOTA, 1,4,7,10-tetraazacyclododecane-1,4,7,10-tetraacetic acid; DO3A, 1,4,7,10-tetraazacyclododecane-1,4,7-tris(*t*-butyl acetate); EDTA, ethylene diamine tetraacetic acid; EPR, enhanced permeation and retention; FDG, fluoro-2-deoxy-2-D-glucose; FPLC, fast protein liquid chromatography; GPC, gel permeation chromatography; IHC, immunohistochemistry; ITLC, instant thin layer chromatography; MRI, magnetic resonance imaging; NMR, nuclear magnetic resonance; NPRA, natriuretic peptide receptor A; NPRC, natriuretic peptide clearance receptor; PCa, prostate cancer; PEG, poly(ethylene glycol); PEGMA,

poly(ethylene glycol) methyl ether mathacrylate; PET, positron emission tomography; RAFT, radical addition−fragmentation transfer; ROI, region of interest; SPECT, single photon emission computed tomography; SUV, standardized uptake value; T/B, tumor-to-blood; T/K, tumor-to-kidney; T/M, tumor-to-muscle

REFERENCES

(1) Siegel, R., Naishadham, D., and Jemal, A. (2012) Cancer statistics, 2012. *CA Cancer J. Clin. 62*, 10−29.

(2) Turkbey, B., Pinto, P. A., and Choyke, P. L. (2009) Imaging techniques for prostate cancer: implications for focal therapy. *Nat. Rev. Urol. 6*, 191−203.

(3) Pinto, F., Totaro, A., Palermo, G., Calarco, A., Sacco, E., D'Addessi, A., Racioppi, M., Valentini, A., Gui, B., and Bassi, P. (2012) Imaging in prostate cancer staging: present role and future perspectives. *Urol. Int. 88*, 125−136.

(4) Ravizzini, G., Turkbey, B., Kurdziel, K., and Choyke, P. L. (2009) New horizons in prostate cancer imaging. *Eur. J. Radiol. 70*, 212−226.

(5) Lawrence, E. M., Gnanapragasam, V. J., Priest, A. N., and Sala, E. (2012) The emerging role of diffusion-weighted MRI in prostate cancer management. *Nat. Rev. Urol. 9*, 94−101.

(6) Bouchelouche, K., Turkbey, B., Choyke, P., and Capala, J. (2010) Imaging prostate cancer: an update on positron emission tomography and magnetic resonance imaging. *Curr. Urol. Rep. 11*, 180−190.

(7) Lears, K. A., Ferdani, R., Liang, K., Zheleznyak, A., Andrews, R., Sherman, C. D., Achilefu, S., Anderson, C. J., and Rogers, B. E. (2011) In vitro and in vivo evaluation of 64Cu-labeled SarAr-bombesin analogs in gastrin-releasing peptide receptor-expressing prostate cancer. *J. Nucl. Med. 52*, 470−477.

(8) Jackson, A. B., Nanda, P. K., Rold, T. L., Sieckman, G. L., Szczodroski, A. F., Hoffman, T. J., Chen, X., and Smith, C. J. (2012) 64Cu-NO2A-RGD-Glu-6-Ahx-BBN(7−14)NH2: a heterodimeric targeting vector for positron emission tomography imaging of prostate cancer. *Nucl. Med. Biol. 39*, 377−387.

(9) Graham, M. M., and Menda, Y. (2011) Radiopeptide imaging and therapy in the United States. *J. Nucl. Med. 52* (Suppl 2), 56S−63S.

(10) Nanda, P. K., Pandey, U., Bottenus, B. N., Rold, T. L., Sieckman, G. L., Szczodroski, A. F., Hoffman, T. J., and Smith, C. J. (2012) Bombesin analogues for gastrin-releasing peptide receptor imaging. *Nucl. Med. Biol. 39*, 461−471.

(11) Chen, Y., Pullambhatla, M., Foss, C. A., Byun, Y., Nimmagadda, S., Senthamizhchelvan, S., Sgouros, G., Mease, R. C., and Pomper, M. G. (2011) 2-(3-{1-Carboxy-5-[(6-[18F]fluoro-pyridine-3-carbonyl)-amino]-pentyl}-ureido)-pen tanedioic acid, [18F]DCFPyL, a PSMA-based PET imaging agent for prostate cancer. *Clin. Cancer Res. 17*, 7645−7653.

(12) Lutje, S., Boerman, O. C., van Rij, C. M., Sedelaar, M., Helfrich, W., Oyen, W. J., and Mulders, P. F. (2012) Prospects in radionuclide imaging of prostate cancer. *Prostate 72*, 1262−1272.

(13) Craft, J. M., De Silva, R. A., Lears, K. A., Andrews, R., Liang, K., Achilefu, S., and Rogers, B. E. (2012) In vitro and in vivo evaluation of a 64Cu-labeled NOTA-Bn-SCN-Aoc-bombesin analogue in gastrin-releasing peptide receptor expressing prostate cancer. *Nucl. Med. Biol. 39*, 609−616.

(14) Liu, Y., and Welch, M. J. (2012) Nanoparticles labeled with positron emitting nuclides: advantages, methods, and applications. *Bioconjugate Chem. 23*, 671−682.

(15) Talekar, M., Kendall, J., Denny, W., and Garg, S. (2011) Targeting of nanoparticles in cancer: drug delivery and diagnostics. *Anticancer Drugs 22*, 949−962.

(16) Kievit, F. M., and Zhang, M. (2011) Cancer nanotheranostics: improving imaging and therapy by targeted delivery across biological barriers. *Adv. Mater. 23*, H217−H247.

(17) Steinmetz, N. F., Ablack, A. L., Hickey, J. L., Ablack, J., Manocha, B., Mymryk, J. S., Luyt, L. G., and Lewis, J. D. (2011) Intravital imaging of human prostate cancer using viral nanoparticles targeted to gastrin-releasing Peptide receptors. *Small 7*, 1664−1672.

(18) Chanda, N., Kattumuri, V., Shukla, R., Zambre, A., Katti, K., Upendran, A., Kulkarni, R. R., Kan, P., Fent, G. M., Casteel, S. W., Smith, C. J., Boote, E., Robertson, J. D., Cutler, C., Lever, J. R., Katti, K. V., and Kannan, R. (2010) Bombesin functionalized gold nanoparticles show in vitro and in vivo cancer receptor specificity. *Proc. Natl. Acad. Sci. U. S. A. 107*, 8760−8765.

(19) Mendoza-Sanchez, A. N., Ferro-Flores, G., Ocampo-Garcia, B. E., Morales-Avila, E., de, M. R. F., De Leon-Rodriguez, L. M., Santos-Cuevas, C. L., Medina, L. A., Rojas-Calderon, E. L., and Camacho-Lopez, M. A. (2010) Lys3-bombesin conjugated to 99mTc-labelled gold nanoparticles for in vivo gastrin releasing peptide-receptor imaging. *J Biomed. Nanotechnol. 6*, 375−384.

(20) Becker, A. L., Orlotti, N. I., Folini, M., Cavalieri, F., Zelikin, A. N., Johnston, A. P., Zaffaroni, N., and Caruso, F. (2011) Redox-active polymer microcapsules for the delivery of a survivin-specific siRNA in prostate cancer cells. *ACS Nano 5*, 1335−1344.

(21) Maack, T. (2006) The broad homeostatic role of natriuretic peptides. *Arq Bras Endocrinol Metabol 50*, 198−207.

(22) Wang, X., Raulji, P., Mohapatra, S. S., Patel, R., Hellermann, G., Kong, X., Vera, P. L., Meyer-Siegler, K. L., Coppola, D., and Mohapatra, S. (2011) Natriuretic peptide receptor a as a novel target for prostate cancer. *Mol. Cancer 10*, 56−67.

(23) Sun, Y., Eichelbaum, E. J., Wang, H., and Vesely, D. L. (2007) Atrial natriuretic peptide and long acting natriuretic peptide inhibit MEK 1/2 activation in human prostate cancer cells. *Anticancer Res. 27*, 3813−3818.

(24) Sun, Y., Eichelbaum, E. J., Lenz, A., Skelton, W. P. t., Wang, H., and Vesely, D. L. (2009) Atrial natriuretic peptide and long-acting natriuretic peptide inhibit ras in human prostate cancer cells. *Anticancer Res. 29*, 1889−1893.

(25) Kong, X., Wang, X., Xu, W., Behera, S., Hellermann, G., Kumar, A., Lockey, R. F., Mohapatra, S., and Mohapatra, S. S. (2008) Natriuretic peptide receptor a as a novel anticancer target. *Cancer Res. 68*, 249−256.

(26) Terada, N., Shimizu, Y., Kamba, T., Inoue, T., Maeno, A., Kobayashi, T., Nakamura, E., Kamoto, T., Kanaji, T., Maruyama, T., Mikami, Y., Toda, Y., Matsuoka, T., Okuno, Y., Tsujimoto, G., Narumiya, S., and Ogawa, O. (2010) Identification of EP4 as a potential target for the treatment of castration-resistant prostate cancer using a novel xenograft model. *Cancer Res. 70*, 1606−1615.

(27) Vesely, B. A., Alli, A. A., Song, S. J., Gower, W. R., Jr., Sanchez-Ramos, J., and Vesely, D. L. (2005) Four peptide hormones' specific decrease (up to 97%) of human prostate carcinoma cells. *Eur. J. Clin. Invest. 35*, 700−710.

(28) Shokeen, M., Pressly, E. D., Hagooly, A., Zheleznyak, A., Ramos, N., Fiamengo, A. L., Welch, M. J., Hawker, C. J., and Anderson, C. J. (2011) Evaluation of multivalent, functional polymeric nanoparticles for imaging applications. *ACS Nano 5*, 738−747.

(29) Pressly, E. D., Rossin, R., Hagooly, A., Fukukawa, K., Messmore, B. W., Welch, M. J., Wooley, K. L., Lamm, M. S., Hule, R. A., Pochan, D. J., and Hawker, C. J. (2007) Structural effects on the biodistribution and positron emission tomography (PET) imaging of well-defined (64)Cu-labeled nanoparticles comprised of amphiphilic block graft copolymers. *Biomacromolecules 8*, 3126−3134.

(30) Nagabhushan, M., Miller, C. M., Pretlow, T. P., Giaconia, J. M., Edgehouse, N. L., Schwartz, S., Kung, H. J., de Vere White, R. W., Gumerlock, P. H., Resnick, M. I., Amini, S. B., and Pretlow, T. G. (1996) CWR22: the first human prostate cancer xenograft with strongly androgen-dependent and relapsed strains both in vivo and in soft agar. *Cancer Res. 56*, 3042−3046.

(31) Dyke, J. P., Zakian, K. L., Spees, W. M., Matei, C., Chen, Y., Mao, X., Shungu, D. C., and Koutcher, J. A. (2003) Metabolic response of the CWR22 prostate tumor xenograft after 20 Gy of radiation studied by 1H spectroscopic imaging. *Clin. Cancer Res. 9*, 4529−4536.

(32) Roe, K., Mikalsen, L. T., van der Kogel, A. J., Bussink, J., Lyng, H., Ree, A. H., Marignol, L., and Olsen, D. R. (2012) Vascular responses to radiotherapy and androgendeprivation therapy in experimental prostate cancer. *Radiat. Oncol. 7*, 75.

(33) Ponde, D. E., Dence, C. S., Oyama, N., Kim, J., Tai, Y. C., Laforest, R., Siegel, B. A., and Welch, M. J. (2007) 18F-fluoroacetate: a potential acetate analog for prostate tumor imaging–in vivo evaluation of 18F-fluoroacetate versus 11C-acetate. *J. Nucl. Med. 48*, 420−428.
(34) McCarthy, D. W., Shefer, R. E., Klinkowstein, R. E., Bass, L. A., Margeneau, W. H., Cutler, C. S., Anderson, C. J., and Welch, M. J. (1997) Efficient production of high specific activity 64Cu using a biomedical cyclotron. *Nucl. Med. Biol. 24*, 35−43.
(35) Herrero, P., Kim, J., Sharp, T. L., Engelbach, J. A., Lewis, J. S., Gropler, R. J., and Welch, M. J. (2006) Assessment of myocardial blood flow using 15O-water and 1−11C-acetate in rats with small-animal PET. *J. Nucl. Med. 47*, 477−485.
(36) Liu, Y., Ibricevic, A., Cohen, J. A., Cohen, J. L., Gunsten, S. P., Frechet, J. M., Walter, M. J., Welch, M. J., and Brody, S. L. (2009) Impact of hydrogel nanoparticle size and functionalization on in vivo behavior for lung imaging and therapeutics. *Mol. Pharmaceutics 6*, 1891−1902.
(37) Almutairi, A., Rossin, R., Shokeen, M., Hagooly, A., Ananth, A., Capoccia, B., Guillaudeu, S., Abendschein, D., Anderson, C. J., Welch, M. J., and Frechet, J. M. (2009) Biodegradable dendritic positron-emitting nanoprobes for the noninvasive imaging of angiogenesis. *Proc. Natl. Acad. Sci. U. S. A. 106*, 685−690.
(38) Liu, Y., Abendschein, D., Woodard, G. E., Rossin, R., McCommis, K., Zheng, J., Welch, M. J., and Woodard, P. K. (2010) Molecular imaging of atherosclerotic plaque with (64)Cu-labeled natriuretic peptide and PET. *J. Nucl. Med. 51*, 85−91.
(39) Liu, Y., Pressly, E. D., Abendschein, D. R., Hawker, C. J., Woodard, G. E., Woodard, P. K., and Welch, M. J. (2011) Targeting angiogenesis using a C-type atrial natriuretic factor-conjugated nanoprobe and PET. *J. Nucl. Med. 52*, 1956−1963.
(40) Rogers, B. E., Bigott, H. M., McCarthy, D. W., Della Manna, D., Kim, J., Sharp, T. L., and Welch, M. J. (2003) MicroPET imaging of a gastrin-releasing peptide receptor-positive tumor in a mouse model of human prostate cancer using a 64Cu-labeled bombesin analogue. *Bioconjugate Chem. 14*, 756−763.
(41) Ting, G., Chang, C. H., and Wang, H. E. (2009) Cancer nanotargeted radiopharmaceuticals for tumor imaging and therapy. *Anticancer Res. 29*, 4107−4118.
(42) Rubattu, S., Sciarretta, S., Morriello, A., Calvieri, C., Battistoni, A., and Volpe, M. (2010) NPR-C: a component of the natriuretic peptide family with implications in human diseases. *J. Mol. Med. (Berlin) 88*, 889−897.
(43) Bergers, G., and Benjamin, L. E. (2003) Tumorigenesis and the angiogenic switch. *Nat. Rev. Cancer 3*, 401−410.
(44) Dudley, A. C. (2012) Tumor endothelial cells. *Cold Spring Harbor Perspect. Med. 2*, a006536.